Measuring Ozone and Aerosol Optical Depth with a Solar Spectrophotometer

Adam T. Whitten

2009

Introduction

Sunlight impinging at the top of the earth's atmosphere is subject to absorption and scattering as it makes its way to the surface. The net irradiance for a particular wavelength, L_λ, at the surface is described by the Beer-Lambert Law [*Slusser et al.*, 2000]:

$$L_\lambda = L_{\lambda 0} D^{-2} \exp\left(-u_{\lambda\infty} \sec\theta\right) \qquad u_{\lambda\infty} = \int_0^\infty \sigma_\lambda \, \rho(z) \, dz$$

where $L_{\lambda 0}$ is the irradiance at the top of the earth's atmosphere (also called air mass zero or AM0); D^{-2} is the earth to sun distance in astronomical units (AU); θ is the solar zenith angle; $u_{\lambda\infty}$ is the optical thickness of the atmosphere; σ_λ is the extinction coefficient; and $\rho(z)$ is the density of the scatterer or absorber.

The extinction coefficient can be separated into quantities that represent absorption, molecular scattering, and aerosol scattering:

$$u_{\lambda\infty} = \int_0^\infty \alpha \, \rho_{abs}(z) \, dz + \int_0^\infty \beta \, \rho(z) \, dz + \int_0^\infty \delta_{aer} \, \rho_{aer}(z) \, dz$$

where α is the absorption coefficient of the absorbing species; β is the molecular (Rayleigh) scattering coefficient for the atmosphere; and δ_{aer} is the aerosol (Mie) scattering coefficient. Note that the denstity profiles for absorbers and aerosol scatterers will in general be different from the density profile of the atmosphere as a whole.

Assuming that the coefficients are path independent, the above integrals involve only the density integrated over the entire atmosphere giving [*London*, 1985]:

$$L_\lambda = L_{\lambda 0} D^{-2} \exp\left(-\alpha X \mu - \beta m P/P_0 - \delta m'\right) \tag{1}$$

where X is the total amount of absorber in a vertical column at STP; μ is the ratio of the actual and vertical paths through the absorbing layer; m is the optical path length allowing for refraction; P is the station pressure; P_0 is the mean sea level pressure; δ is the aerosol optical depth; and m' is $\sec\theta$ where θ is the solar zenith angle. To use this expression appropriate units for α (cm^{-1}) and β (atm^{-1}) must be used (δ is dimensionless).

The solar zenith angle is calculated using the relationship [*Komhyr*, 1980]:

$$\cos\theta = \sin\phi \sin\delta + \cos\phi \cos\delta \cos h$$

where ϕ is the latitude; h is the hour angle given by $h = 15^\circ(12 - t)$ with t equal to the local time; and δ is the solar declination given by $\delta = -23.4^\circ \cos[360^\circ(t_j + 10)/365]$ with t_j equal to the Julian Date or day number.

The ratio of the actual and vertical paths through the absorbing material is calculated from [*Komhyr*, 1980]:

$$\mu = \frac{R+h}{\sqrt{(R+h)^2 - (R+r)^2 \sin^2\theta}}$$

where R is the mean radius of the earth; r is the height of the measuring station above sea level; h is the height of the absorbing layer above sea level; and θ is the solar zenith angle.

The optical path length for a molecular scattering atmosphere allowing for refraction is [*Komhyr*, 1980]:

$$m = m' - 0.0018167(m'-1) - 0.002875(m'-1)^2 - 0.0008083(m'-1)^3$$

where again m' is $\sec\theta$ and θ is the solar zenith angle.

To investigate atmospheric absorption by a chemical species such as ozone, spectrophotometry relies on making measurements at narrow wavelength intervals that are strongly absorbed (L_a) and weakly absorbed (L_b) by a particular gas (called a wavelength pair). To minimize the effects of aerosol scattering measurements at a second wavelength pair (L_c, L_d) can also made. Then to find the amount of the absorber the Beer-Lambert equation can be rearranged giving an expression appropriate to use for ozone measurements at ultaviolet wavelengths:

$$X = \frac{\ln\left(\frac{L_{a0}L_b}{L_{b0}L_a}\right) - \ln\left(\frac{L_{c0}L_d}{L_{d0}L_c}\right) - \left[(\beta_a - \beta_b) - (\beta_c - \beta_d)\right] m \frac{P}{P_0}}{\left[(\alpha_a - \alpha_b) - (\alpha_c - \alpha_d)\right]\mu} \tag{2}$$

where the term $\left[(\delta_a - \delta_b) - (\delta_c - \delta_d)\right] m' \approx 0$ is ignored [*Komhyr*, 1980]. Note that the earth sun distance dependency (D) vanishes when measurements at two wavlengths are subtracted in this manner.

To determine the aerosol optical depth, Equation (1) can be solved for δ:

$$\delta = \frac{\ln\left(\frac{L_0}{LD^2}\right) - \alpha X \mu - \beta m \left(\frac{P}{P_0}\right)}{m'} \tag{3}$$

For wavelengths for which there is no significant absorption ($\alpha \approx 0$) the Beer-Lambert Law can be rewritten to give information about aerosol scattering coefficients:

$$\delta = \frac{\ln\left(\frac{L_0}{LD^2}\right) - \beta m \left(\frac{P}{P_0}\right)}{m'}$$

Aerosols scatter red light more than blue light and the amount of scattering in the red increases with aerosol diameter. Therefore a color ratio defined as $\delta_{\text{blue}}/\delta_{\text{red}}$ would be $\gg 1.0$ for large aerosols and closer to unity for small aerosols.

Instrument

The instrument uses ten photodiodes with filters to measure irradiances at ten different wavelengths. Photodiodes with filters for the ultraviolet range are provided by Boston Electronics and have an active area of 0.0625 mm^2. Photodiodes for the visible and infrared ranges are provided by Intor Optics and have an active area of 3.08 mm^2. The photodiodes are mounted in a 30 cm long cylindrical tube of diameter 3.75 cm giving an acceptance angle for incoming radiation of $\sim 3.6^\circ$ from the longitudinal axis of the instrument. The photodiodes are connected in photovoltaic mode (see Figure 1) to high precision Burr-Brown Difet® opamps. Specifications for the photodiodes are listed in Table 1.

The output voltages are digitized by the 12-bit ($\pm$1/4 LSB) A/D converter that is part of the Microchips PIC16C774 microcontroller. The microcontroller also queries an Axiom Sandpiper II

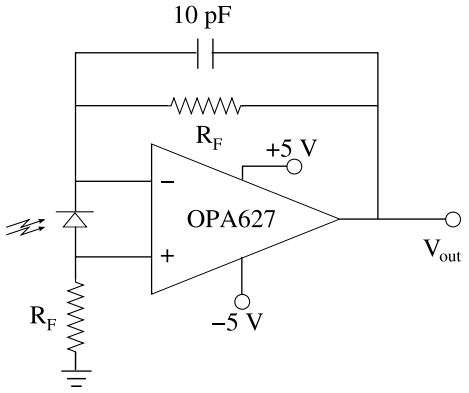

Figure 1: Photodiode opamp circuit.

Table 1: Photodiode/filter specifications

Photodiode	**UVC**	**UVB**	**UVA**	**Violet**	**Blue**
Peak λ (nm)	265	315	340	440	500
FWHM (nm)	30	30	50	10	10
R_F $\pm$1%	1 GΩ	100 MΩ	10 MΩ	100 kΩ	100 kΩ
Photodiode	**Red**	**IR1**	**IR2**	**IR3**	**IR4**
Peak λ (nm)	675	870	930	940	1020
FWHM (nm)	10	10	10	10	15
R_F $\pm$1%	10 kΩ	100 kΩ	100 kΩ	75 kΩ	100 kΩ

GPS for RMC data before each reading of the irradiances. All data is stored in serial EEPROM in typical datalogging fashion. Data is retrieved from the datalogger by connecting it to a reader that transfers it from the datalogger to a computer. The useful data set consists of UTC time, UTC date, latitude, longitude, and ten numbers from 0-4095 which represent the digitized voltages from the photodiode/opamp circuits. Pressure is retrieved from the NOAA/ESRL radiosonde database.

After initial operation some refinements were made to the instrument. The physical location of the diodes within the tube was rearranged on June 16, 2008 in order to bring them closer to longitudinal axis – this makes aligning the instrument with the sun easier, since a slight misalignment will no longer put any of the photodiodes in partial shadow. Feedback resistors for the 440, 500, 675, 930, 940, and 1020 nm channels were reduced on February 1, 2009 in order to reduce the possibility of op amp saturation. Table 1 shows the current values.

Calibration

A spectrophotometer that measures voltages proportional to the irradiance can make use of the Beer-Lambert Law rewritten in terms of the voltages if the voltage the instrument would read at the top of the earth's atmosphere is known [*Schmid and Wehrli*, 1995]. This requires calibration of the instrument to determine its response as a function of decreasing air mass. Ground-based calibration methods usually take repeated measurements at changing solar zenith angles and then fit the logarithm of the voltage versus the secant of the solar zenith angle (m) to a straight line.

$$\ln(V_\lambda D^2) = \ln V_{\lambda 0} - u_\lambda m$$

The y-intercept corresponds to the instrument reading for air mass zero (AM0) which is interpreted as the top of the atmosphere at an earth sun distance of 1 AU. The slope is interpreted as the optical thickness of the atmosphere on the day of the calibration. Once the instrument's response at AM0 is known the Beer-Lambert Law is rewritten as:

$$\ln\left(\frac{V_{\lambda 0}}{V_\lambda D^2}\right) = \alpha X \mu + \beta m P/P_0 + \delta \sec\theta \tag{4}$$

Calibrations are made under clear sky conditions when the atmosphere is stable. Some researchers recommend performing calibrations at the top of a mountain to minimize boundary layer effects, but this is not possible at Collegeville, Minnesota. Initial calibrations were performed on August 14 and 15, 2006. Each reading represents the average of ten measurements for a particular solar zenith angle taken at the campus of St. John's University in Collegeville, Minnesota. Uncertainties for each data point are given by the standard error of the mean. After physical rearrangement of the diodes was made a new calibration was performed on May 28, 2009. Each reading represents the average of twenty measurements with uncertainties given by the standard deviation of the mean.

Figure 2 shows the raw calibration data for the UV-B and UV-A channels plotted as $\ln(V)$ versus m, where m corresponds to the secant of the solar zenith angle or equivalently the air mass. The August 2006 calibration contains data from 9:00-16:00 on August 14 and 7:30-12:00 on August 15. The long time periods introduce variations due changing air masses, especially variations that occur within the boundary layer. The July 2007 calibration contains data from July 1 (8:20-16:50), July 4 (9:30-13:00), July 8 (7:00-12:30), July 9 (5:50-15:50), July 14 (7:20-13:50), and July 22 (8:00-13:20). Even though the air mass may have been changing over the course of the three weeks of calibrations, the uncertainties in the fit parameters half of those for the 2006 calibration data. The May 2009 calibration contains data from 6:00-12:00 for a single day (May 28) with no measurements past local noon. In addition, only air masses between 2 and 6 were used for the non-UV calibrations [*Slusser et al.*, 2000]. Tables 2 and 3 show the AM0 fit parameters with uncertainty as determined by Mathematica® for the ultraviolet and visible-infrared channels respectively.

Table 2: Fit parameters for UV calibration data.

	August 2006		July 2008		May 2009	
Photodiode λ	$\ln V_{\lambda 0}$	$\delta(\ln V_{\lambda 0})$	$\ln V_{\lambda 0}$	$\delta(\ln V_{\lambda 0})$	$\ln V_{\lambda 0}$	$\delta(\ln V_{\lambda 0})$
315 nm	1.868	0.180	2.234	0.076	2.336	0.133
340 nm	1.058	0.110	1.256	0.053	1.157	0.114

Table 3: Fit parameters for visible and infrared calibration data (May 2009).

Parameter	440 nm	500 nm	675 nm	870 nm	930 nm	940 nm	1020 nm
$\ln V_{\lambda 0}$	0.559	1.503	0.302	2.202	1.904	1.829	1.342
$\delta(\ln V_{\lambda 0})$	0.197	0.146	0.203	0.195	0.176	0.055	0.207

Variations are expected because of fluctuations in the ozone, water vapor, and aerosol content. Being more restrictive in the range of air mass used for calibration improves the fit, but leads to a larger relative uncertainty. This is the source of the correspondingly higher uncertainties for the visible and infrared channels listed in Table 3. It should be noted that on other days for which a calibration was attempted, the Langley plots show a clear change in air mass seen as discontinuities in the plot.

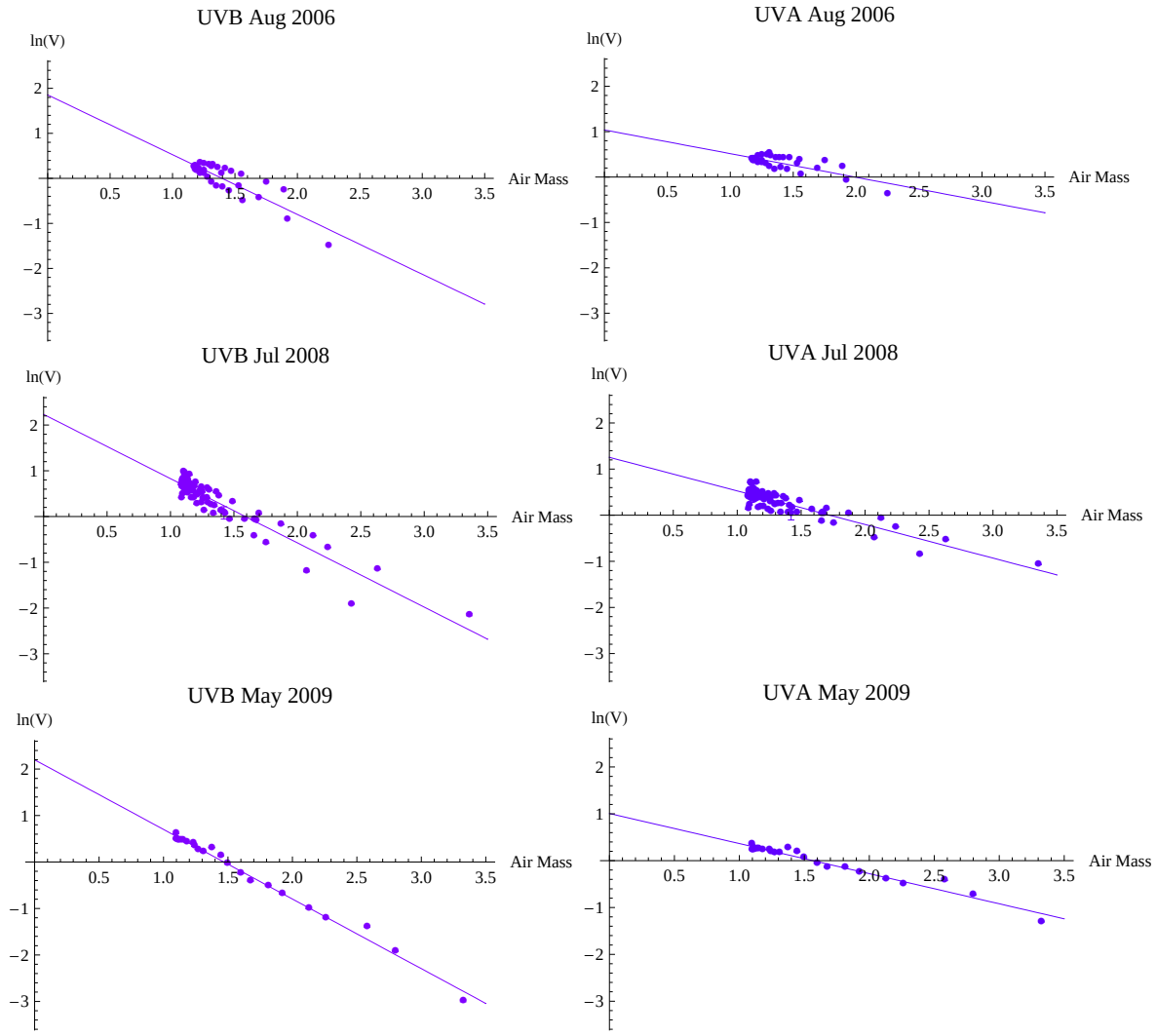

Figure 2: Typical Langley plots for August 2006 (top), July 2008 (middle), and May 2009 (bottom).

Analysis

Table 4 shows the values for the decadic ozone absorption coefficients [*Inn and Tanaka*, 1953] and exponential Rayleigh optical depths [*Bucholtz*, 1995] used to analyze the data. Analysis is performed using base 10 logarithms of the voltages necessitating a conversion of the Rayleigh optical depths. They are divided by $\ln 10$ before use in calculations.

Ozone

It was hoped that the large bandpass of the 265 nm detector would allow it to be used to detect ultraviolet radition in the lower end of the UVB range. After the first calibration it became apparent that data from the 265 nm detector would not be usable. While the signal from the UVC detector follows the same trend as those form the UVB and UVA detectors, strong absorption by ozone and thermal noise in the requisite large feedback resistor combine to make it useful only for qualitative observations. Therefore, preliminary analysis of ozone was performed using a single wavelength pair (315 nm and 340 nm). While this means there may be some unknown contribution to the signal from aerosol scattering, the overall trend in daily values is similar to that seen in data from NASA's Ozone Monitoring Instrument [*Ozone Processing Team*, 2006].

Table 4: Ozone absorption coefficients α and Rayleigh optical depths β.

Photodiode	**UVC**	**UVB**	**UVA**	**Violet**	**Blue**
Peak λ (nm)	265	315	340	440	500
α **(cm^{-1})**	116.3	0.6205	0.02474	0.002381	0.01667
β **(atm^{-1})**	2.1020	0.98975	0.71300	0.24290	0.14350
Photodiode	**Red**	**IR1**	**IR2**	**IR3**	**IR4**
Peak λ (nm)	675	870	930	940	1020
α **(cm^{-1})**	0.01667	0.002381	0.002381	0.002381	0.002381
β **(atm^{-1})**	0.042285	0.015619	0.011841	0.011384	0.0089460

Level 3 gridded data is a weighted average of geographical areas (1.00° lat. by 1.00° lon.) with total uncertainties of up to 5.6% [*McPeters et al.*, 2006]. Each SPM data point is usually the average of 10 measurements taken over a 100 second interval (10 seconds between measurements) with an uncertainty given by the standard error of the mean. On occasion an average of as few as 3 or as many as 20 measurements are used. Most SPM measurements were made close to noon (local standard time), although on some days multiple measurements were made. However, the uncertainties in the SPM ozone levels are dominated by the uncertainties in the calibration constants given in Table 2. Figure 3 shows ozone values from Level 3 gridded OMI data displayed as a solid blue line and from the spectrophotometer (SPM) displayed as a dashed red line.

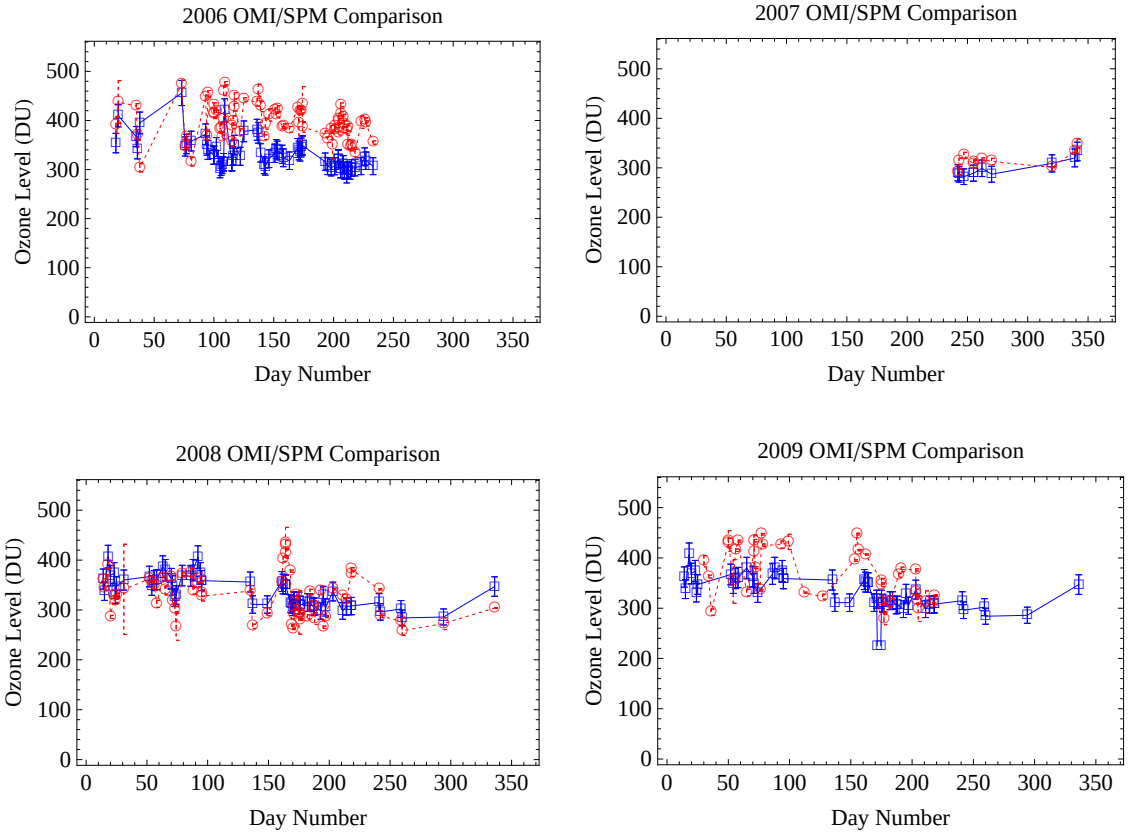

Figure 3: Ozone trend comparisons. OMI data is in blue and SPM data is in red.

Aerosol Optical Depth

Aerosol optical depths at 440 nm, 500 nm, 675 nm, 870 nm, 930 nm, 940 nm, and 1020 nm were calculated beginning in February 2009 using Equation (4). The column ozone calculated from the UVB and UVA channels was accounted for, but since ozone absorption at the visible and infrared wavelengths is very small ozone has a negligible effect.

Graphs of optical depth versus day number are shown in Figure 4. All channels show similar behavior before the month of June, after which trends in the optical depths differ: for visible wavelength channels (440 nm, 500 nm, and 675 nm) the optical depth remains relatively constant at the beginning of June, then drops during the last week of June, and recovers after the first week of July; for the 870 nm and 1020 nm wavelength channels optical depths steadily decrease in June and increase in July; for the 930 nm and 940 nm wavelength channels optical depths increase in June, decrease at the beginning of July, and then increase again.

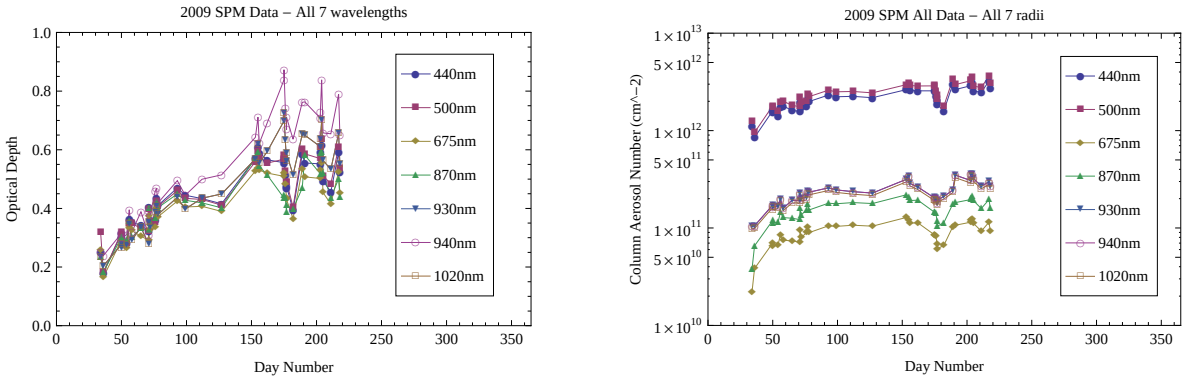

Figure 4: Aerosol optical depths (left) and column aerosol number density from Eq. 5 (right).

The 930 nm and 940 nm wavelength channels are affected by water vapor absorption and 936 nm, whereas the other channels should be unaffected by any water vapor. Therefore, the differences in the optical depths during June could be do to an increase in wator vaper in the atmosphere. The optical depths at 440 nm, 500 nm, 675 nm, 870 nm, and 1020 nm are interpreted as the aerosol optical depths and are use to reconstruct the columnar aerosol number density following the method of *Grassl*, 1971.

This iterative method invloves inverting the general expression for optical depth

$$\tau_\lambda = \pi \int_{r_1}^{r_2} Q(r,\lambda)\, n(r)\, r^2\, dr \tag{5}$$

to obtain $n(r)$. $Q(r,\lambda)$ is the extinction efficiency and is calculated from Mie theory. The interval r_1 to r_2 is specific for each wavelength channel of the spectrophotometer and is chosen as follows: the Mie calculation, $Q(r,\lambda)$, has a first local maximum of approximately 4 and the range of r for which $Q \geq 3$ around this maximum was chosen to define r_1 and r_2 for each wavelength channel. An initial lognormal size distribution is calculated for each wavelength interval centered around the value $\bar{r} = \sqrt{r_1^2 + r_2^2}$ since the optical depth depends on r^2. These values are summarized in Table 5.

Optical depths, $\tau_{\lambda,c}$, are calculated from the initial distribution, $n_{0,\lambda}(r)$, and compared to the measured optical depth, $\tau_{\lambda,m}$. If the magnitude of their difference is greater than the uncertainty in the measured optical depth then the distribution is adjusted using a simple ratio $n_\lambda(r) = (\tau_{\lambda,m}/\tau_{\lambda,c})\ n_{0,\lambda}(r)$. Since the radii ranges for each wavelength channel overlap, many iterations

Table 5: Radii ranges used columnar aerosol number density calculations.

Wavelength	440 nm	500 nm	675 nm	875 nm	930 nm*	940 nm*	1020 nm
r_1 (μm)	0.187	0.213	0.287	0.370	0.396	0.400	0.434
r_2 (μm)	0.418	0.475	0.640	0.825	0.882	0.892	0.967
$\bar{r}$ (μm)	0.324	0.368	0.496	0.639	0.684	0.691	0.749

*Note: the 930 nm and 940 nm are not used for the determination of $n(r)$.

must be performed before the process converges to a solution (in practice, less than 30 iterations are required).

Once $n(r)$ is determined $\tau_{\lambda,c}$ is calculated using Equation 5 for the 930 nm and 940 nm channels. These distributions are nearly identical which is expected since their $\bar{r}$ values differ by only 7 nm. The extinction due to absorption by water vapor, $\tau_{\lambda,a}$, is found by subtraction: $\tau_{\lambda,a} = \tau_{\lambda,m} - \tau_{\lambda,c}$. Figure 4 shows calculated values of $n(\bar{r})$ which can be interpreted as representing a bimodal lognormal distribution.

References

Bucholtz, A. (1995), Rayleigh-scattering calculations for the terrestrial atmosphere, *Appl. Opt., 34*(15), 2765-2773.

Grassl, H. (1971), Determination of aerosol size distributions from spectral attenuation measurements, *Appl. Opt., 10*(11), 2534-2538.

Ichoku, C., R. Levy, Y. J. Kaufman, L. A. Remer, R.-R. Li, V. J. Martins, B.N. Holben, N. Abuhassan, I. Slutsker, T. F. Eck, and C. Pietras (2002), Analysis of the performance characteristics of the five-channel Microtops II Sun photometer for measuring aerosol optical thickness and precipatable water vapor, *J. Geo. Res., 107*(D13), 4179-4195.

Inn, E. C. Y. and Y. Tanaka (1953), Absorption coefficient of ozone in the ultraviolet and visible regions, *J. Opt. Soc. of Am., 43*(10), 870-873.

King, M. D., D. M. Byrne, B.M. Herman, and J. A. Reagan (1978) Aerosol size distributions obtained by inversion of spectral optical depth measurements, *J. Atmos. Sci.*, 35, 2153-2167.

Komhyr, W. D. (1980), Operations handbook – ozone observations with a Dobson spectrophotometer, *WMO Global Ozone Research and Monitoring Project Rep. 6*, World Meteorological Organization, Geneva, Switzerland.

London, J. (1985). The observed distribution of atmospheris ozone and its variations, in *Ozone in the Free Atmosphere*, edited by R. C. Whitten and S. S. Prasad, pp. 11-80, Van Nostrand Reinhold, New York, N. Y.

McPeters, R. D., P. K. Bhartia, A. J. Kruger, J. R. Herman, C. G. Wellemeyer, C. J. Seftor, G. Jaross, O. Torres, L. Moy, G. Labow, W. Byerly, S. L. Taylor, T. Swissler, and R. P. Cebula (1998), *Earth Probe Total Ozone Mapping Spectrometer (TOMS) Data Products User's Guide*, NASA Goddard Space Flight Center, Greenbelt, Maryland.

Ozone Processing Team (2006), Total Ozone Mapping Spectrometer, NASA/GSFC Code 613.3, Goddard Space Flight Center, Greenbelt, Maryland.

Rothman, L.S., I.E. Gordon, A. Barbe, D. ChrisBenner, P.F. Bernath, M. Birk, V. Boudon, L.R. Brown, A. Campargue, J.-P. Champion, K. Chance, L.H. Coudert, V. Danaj, V.M. Devi, S. Fally, J.-M. Flaud, R.R. Gamache, A. Goldmanm, D. Jacquemart, I. Kleiner, N. Lacome, W.J. Lafferty, J.-Y. Mandin, S.T. Massie, S.N. Mikhailenko, C.E. Miller, N. Moazzen-Ahmadi, O.V. Naumenko, A.V. Nikitin, J. Orphal, V.I. Perevalov, A. Perrin, A. Predoi-Cross, C.P. Rinsland, M. Rotger, M. Šimečková, M.A.H. Smith, K. Sung, S.A. Tashkun, J. Tennyson, R.A. Toth, A.C. Vandaele, J. VanderAuwera (2009), The *HITRAN* 2008 molecular spectroscopic database, *J. of Quant. Spect. & Rad. Trans., 110*, 533-572.

Schmid, B. and C. Wehrli (1995), Comparison of Sun photometer calibration by use of the Langley technique and the standard lamp, *Appl. Opt., 34*(21), 4500-4512.

Slusser, J., J. Gibson, D. Bigelow, D. Kolinski, P. Disterhoft, K. Lantz, and A. Beaubien (2000), Langley method of calibrating UV filter radiometers, *J. Geo. Res., 105*(D4), 4841-4849.